Applied Catalysis B: Environmental 248 (2019) 441–449

Contents lists available at ScienceDirect

Applied Catalysis B: Environmental

journal homepage: www.elsevier.com/locate/apcatb

Significantly accelerated PEC degradation of organic pollutant with addition of sulfite and mechanism study

Aziz-Ur-Rahim Bacha[a], Hanyun Cheng[a], Jin Han[a], Iqra Nabi[a], Kejian Li[a], Tao Wang[a], Yang Yang[a], Saira Ajmal[a], Yangyang Liu[a], Liwu Zhang[a,b,*]

[a] Shanghai Key Laboratory of Atmospheric Particle Pollution and Prevention, Department of Environmental Science & Engineering, Fudan University, Shanghai, 200433, People's Republic of China
[b] Shanghai Institute of Pollution Control and Ecological Security, Shanghai, 200092, People's Republic of China

ARTICLE INFO

Keywords:
PEC
$BiVO_4$
Na_2SO_3
Methyl orange

ABSTRACT

Visible-light-driven photoelectrochemical (PEC) catalysis has been widely studied as a promising technique for the degradation of organic pollutants in wastewater. Herein, we report a sulfite-enhanced PEC degradation process for the degradation of organic pollutant. The degradation rate was significantly enhanced by ~30 times with the addition of 16 mM sulfite. The Electron Spin Resonance (ESR), Transient Absorption (TA) and hole scavenger studies showed that sulfite radicals ($SO_3^{\bullet-}$) were the main reactive species in the reactions. The pollutant degradation pathway was studied by *in-situ* techniques and mass spectrometer, showing that the sulfite addition can promote the cleavage of aromatic ring C—C bond and C—N bond.

1. Introduction

Water is an essential element for all living organisms, due to its unique properties it is important for our planet and also it has a self-cleaning capability through a natural water cycle. Wastewater from industries has become a common threat for living organism and environment. The wastewater from industries contains both organic and inorganic pollutants [1,2]. From estimation, about 15% of dyes were discharged directly as an effluent without any treatment [3]. The careless handling of wastewater from industries, household and hospitals severely affect the quality of the aquatic and terrestrial environment [4]. These effluents are harmful, non-biodegradable and cause severe health threats. The removal of organic dyes is the most critical step in wastewater treatment because they are not degradable by physicochemical treatment methods [2]. The organic dyes such as methyl orange (MO) is the major pollutants that are harmful to the environment and also cause many other health problems [5–7]. Methyl Orange have a bright color due to the presence of azo bond (—N═N—) [8]. The removal of colorful pollutant from wastewater is often more necessary than colorless pollutant because the amount of dyes is distinctly visible and effect on the water environment [9]. Therefore, it is important to find an effective treatment method for wastewater in order to remove the color and degrade the organic pollutants. Recently different physicochemical and oxidative technologies are used for the removal of organic pollutants such as adsorption [10], biodegradation [11], electrochemical oxidation [12,13], reverse osmosis [14], heterogenesis photocatalysis [15,16], sedimentations [17] and sonolysis [18] etc. Nowadays a lot of effort has been done for the photocatalytic degradation of MO under UV or visible light irradiation. The PEC degradation of MO under UV or visible light is the most convenient environmental cleansing method instead of conventional biological treatment processes. PEC is an advanced chemical oxidation process for the degradation of organic pollutants and is more favorable because it has the combined advantages of both photocatalysis and electrochemistry. The applied electric field gives a bias potential to photoanode, the carriers transfer is easier and it quashes the photogenerated electron-hole recombination. These electron and holes are useful to the formation of reactive species for the facilitate degradation of organic pollutants [19–21].

TiO_2 has been widely used as the model photocatalysis system but the application of TiO_2 in water treatment is hindered due to its wide band gap (3.2 eV) [22–24] and rapid photoinduced carriers recombination [25]. Various modifications have been made to solve this problem [26,27]. BiOBr is also used for photocatalytic degradation of MO, it has a band gap (2.7 eV) narrower than TiO_2 [28]. The UV light is only made up of about 4% of the solar spectrum while 40% of solar

* Corresponding author at: Shanghai Key Laboratory of Atmospheric Particle Pollution and Prevention, Department of Environmental Science & Engineering, Fudan University, Shanghai, 200433, People's Republic of China.
E-mail address: zhanglw@fudan.edu.cn (L. Zhang).

https://doi.org/10.1016/j.apcatb.2019.02.049
Received 20 November 2018; Received in revised form 15 January 2019; Accepted 18 February 2019
Available online 20 February 2019
0926-3373/

energy is approximately in the visible region [29]. At the same time, many research efforts have been done to find the best novel visible light active photocatalysts [30–33]. While finding the best novel visible light active photo-catalysts, bismuth vanadate ($BiVO_4$) is known as an important semiconductor due to its unique properties such as ferroelasticity, ionic conductivity, and non-toxicity [34,35]. $BiVO_4$ have a narrow band gap (2.4 eV) and has been considered as one of the most promising photoanode candidates for water splitting and also have the outstanding ability for organic pollutant degradation under visible light irradiation [36–38]. It has a high oxidation ability and excellent stability for oxidation degradation.

Sulfite is mainly produced from flue gas desulfurization and sulfur dioxide is a major air pollutant [39]. Sulfite is mostly used as a hole scavenger and it increases the electron-hole pairs separation produced by the semiconductor [40]. It is recently reported by Li and coworkers that the photocatalytic degradation of organic pollutants can be promoted by sulfite addition [41], sulfite radicals are reactive species for the degradation of pollutants. However, there is still argument over the reactive species [42] the mechanism is still not understood. A direct measurement or evidence of the generation of sulfite radicals is thus greatly desired.

Herein, we have established a novel approach for the beneficial use of sulfite for the degradation of water pollutant MO by using $BiVO_4$ nanoporous film via PEC process. The Electron Spin Resonance (ESR), Transient Absorption (TA) and hole scavenger's studies are employed to investigate the reactive species such as sulfite radicals ($SO_3^{\bullet -}$) and hydroxyl radicals ($^{\cdot}OH$). We systematically investigated the effect of sulfite, the reactive species, illumination time, applied bias, degradation pathway and mechanism of the degradation of methyl orange. This work shows clear evidence of the formation of sulfite radical as reactive species and provides a new cost-effective and sustainable method for the beneficial use of air pollutants for the removal of water pollutants.

2. Materials and methods

2.1. Materials

Bismuth Nitrate Penta-Hydrate ($Bi(NO_3)_3{\cdot}5H_2O$) was purchased from Aladdin Industrial Corporation (Shanghai, China) and Vanadium Oxide (V_2O_5) from Alfa Aesar (China). Ethylenediaminetetraacetic Acid (EDTA), Isopropyl Alcohol (IPA), Hydrochloric Acid (HCl), Methyl Orange (MO) and Sodium Sulfite anhydrous (Na_2SO_3) were obtained from Sinopharm Chemical Reagent Co., Ltd (China). Fluoride-tin oxide (FTO) glasses (size 50 × 10 mm^2, thickness 1 mm) were purchased from Wuhan Jinge-solar Energy Technology Co., Ltd and FTO were sonicated by immersing in the acetone, ethanol, and Deionized (DI) water in sequence to remove the impurities that existed in the surface of the FTO glasses. All chemical reagents were analytical grade and used without any further purification. DI water was used throughout the whole experiment.

2.2. Synthesis of photocatalyst $BiVO_4$

The $BiVO_4$/FTO nanoporous was prepared by drop coating the $BiVO_4$ precursor solution onto the conducting side of the FTO glass. For the $BiVO_4$ precursor solution, 4 mmol of Diethylenetriaminepentaacetic Acid (DTPA) and 1.5 mL ammonia in water (13.0 mol L^{-1}) was added to 40 mL of hot DI water. After dissolving in solute, 2 mmol of Bi $(NO_3)_3.5H_2O$, 0.97 mmol of V_2O_5 powder were added. The resulting mixture was stirred and heated at 80 ℃ to promote the dissolution and reaction until the mixture turned into a transparent solution. By using a pipette, the $BiVO_4$ precursor (40 μL) was dropped on the surface of FTO film. It was left in the oven for dry at 60 ℃, after that the $BiVO_4$ catalysts were calcined at 500 ℃ for 3 h with a ramping rate of 2 ℃ min^{-1}.

2.3. Characterization of photocatalyst $BiVO_4$

For identifying the distinctive nature of microstructure prepared $BiVO_4$ photoelectrode was analyzed by using the field emission scanning electron microscopy (FESEM, Hitachi S-4800, Japan). To find the crystal structure of prepared $BiVO_4$ electrode X-ray diffraction (XRD) patterns study was done, it was obtained with a Bruker instrument and the Cu Kα radiation value ranges from 15° to 70°. UV–vis spectrophotometer (SHIMADZU UV-2600) with an integrating sphere attachment was used for finding the UV spectrum of the prepared $BiVO_4$ electrode. X-ray photoelectron spectroscopy (XPS) was carried out on a Perkin-Elmer PHI-5000C ESCA system which is equipped with a dual X-ray source, Mg Kα (1253.6 eV) anode and a hemispherical energy analyzer were used. The measurement of Linear Sweep Voltammetry (LSV) was done by using the electrochemical station (CHI 660E, Shanghai Chenhua Co., Ltd. China).

2.4. Experiments of photo-electrocatalytic degradation

The potentiostat (CHI 660E, Shanghai Chenhua Co. Ltd. China) was used for the PEC degradation experiment of MO. A 300 W Xe-lamp with AM 1.5 G filter (100 $mWcm^{-2}$) was used as a source of light. The light was irradiated from the back side of the prepared $BiVO_4$/FTO film. Pt wire was used as a counter electrode and the synthesized $BiVO_4$/FTO film (photoanode) was used as the working electrode. The distance between the reactor cell and the light source was 6 cm.

During the PEC process, azo dye methyl orange (MO, 10 ppm) was studied as a model pollutant, and Na_2SO_3 (16 mM) was used as the electrolyte. A certain amount of Na_2SO_3 was added in 40 mL (10 ppm) of MO solution and HCl was added to keep the initial pH of the solution at 7.5, Ohaus (STARTER 2100) was used in the whole experiment for monitoring the pH of the solution. The UV–vis Spectrophotometer (SHIMADZU UV-2600) was used to measure the absorption spectra and quantify MO in the solution. Before reaction, adsorption/desorption equilibrium was reached by stirring the solution in the PEC cell at 400 rpm in dark for 30 min. High-pressure liquid chromatography (HPLC) was performed on LC-10AD (SHIMADZU) to monitor the degradation of MO. All samples were separated by using the Zorbax SB C18 (4.6 mm × 150 mm, 5 μm) reverse phase column at 25 ℃ and the mobile phase consisted of methanol/water = 50:50 (V/V) with a flow rate of 0.8 mL/min and a detection wavelength of 254 nm.

For analysis of intermediates that are formed during MO degradation, Agilent 6540 Q-Tof Micro Liquid Chromatography–Mass Spectroscopy (Q-Tof LC–MS) was used. The Q-Tof LC–MS was equipped with a C18 column (Agilent EP C18, 50 × 2.1 mm). Methanol and water 70:30 (vol /vol) were used as the mobile phase at a flow rate of 0.25 mL/min. The injected sample had a volume of 25 μL.

2.5. Detection of active species

For identifying the relevant active species that produced in the $BiVO_4$/MO/Sulfite solution different types of scavengers were added. For holes or hydroxyl radical's different scavengers like EDTA and isopropyl alcohol (IPA) were used, and for aqueous electron scavenger, the sodium nitrate was used.

2.6. Electron spin resonance (ESR)

Sulfite radicals ($SO_3^{\bullet -}$) and hydroxyl radical ($^{\cdot}OH$) were analyzed by ESR with 5,5-dimethyl-1-pyrroline-oxide (DMPO) as a spin trapper. ESR analysis was done at room temperature on an X-band spectrometer with HS resonator. The general instrument settings were 10 mW power microwave, 3.17 − 3.56 × 10^5 receiver gain, 82 ms time constant, 42 s time sweep. The relative intensity of each component of the spectra was also determined.

2.7. Transient absorption (TA)

In order to measure the sulfite radical in the present work, transient absorption spectra were used to study the photochemical process. The transient intermediates were detected by laser flash photolysis, equipped with an Nd: YAG nanosecond laser system (Beamtech Optronics Co., Ltd), a xenon lamp as analyzing light source, a photomultiplier array, a spectrograph, a transient digitizer, and a computer. The laser system operates with the output of 110 mJ@355 nm, with the repetition rate of 10 Hz. Other detailed descriptions were similar to previous work [43]. Transient absorption spectra were the average result of 100 times measurements at 250 nm probe light and analyzed through curve fittings to obtain the lifetimes. For a stronger signal of reactive species, the detected samples were 0.5 M Na_2SO_3 solution and suspension prepared by sonicating the $BiVO_4$ powder in DI water for 30 min. The prepared suspension was then left to settle for 1 h and the supernatant liquid was used for transient absorption spectra measurements.

2.8. DRIFTS experiment

DRIFTS spectra were collected on a Shimadzu Tracer-100 FTIR spectrometer equipped with a high-sensitivity mercury cadmium telluride (MCT) detector cooled by liquid nitrogen. A temperature controller was coupled with the DRIFTS chamber (Praying Mantis Kit, Harrick). For in situ DRIFT measurement, $BiVO_4$ nanoparticles were employed and they were prepared by the following method: the $BiVO_4$ precursor solution was dried for 24 h at 120 ℃ and then calcined at 500 ℃ in a muffle furnace with the heating rate 2 ℃ min^{-1} for 3 h. The acquired solid sample was ground finely, washed with DI water, ethanol 3 times, and then kept it in the oven for 24 h at 60 ℃. 5 mg of MO was then mechanically mixed with 0.15 g $BiVO_4$ powder to form $BiVO_4$/MO sample. 0.1 g Na_2SO_3 was then mechanically mixed with 0.1 g of $BiVO_4$/MO to study the effect of sulfite. The IR spectrum was recorded automatically after every 5 min.

3. Results and discussion

3.1. Structure, morphology and optical properties

The nanoporous microstructure of $BiVO_4$ film was examined by using the scanning electron microscope (SEM), as shown in Fig. 1a. The $BiVO_4$ film is composed of nanoparticles with a diameter of around 200 nm and its nanoporous microstructure was clearly observed. The pore sizes are approximately from 20 nm to 100 nm. Cross-sectional SEM image was used to investigate the thickness of the nanoporous $BiVO_4$ film, the cross-sectional image shows that $BiVO_4$ film has a thickness of approximately 150 nm and this thickness of $BiVO_4$ is highly suitable for photoelectrochemical reactions based on our previous work [39].

The chemical composition and the crystalline structure of $BiVO_4$ were investigated by using X-ray diffraction (XRD), which are shown in Fig. 1b. The result shows that the synthesized $BiVO_4$ film has a highly consistent diffraction peak with the scheelite monoclinic phase (PDF no. 14-0688) characteristic peaks. The sharp peak of $BiVO_4$ indicates that it has good crystallinity. The diffraction peak of FTO was observed due to its highly porous structure and the thin thickness of the $BiVO_4$ film.

The optical properties of the synthesized nanoporous $BiVO_4$ film were studied by the UV–vis diffraction reflection spectroscopy (UV–vis DRS). Fig. 1c shows that the $BiVO_4$ electrode shows three broad absorption bands at wavelengths of 200–350 nm, 350–450 nm, and 450–500 nm, respectively. Results show that in the visible light region ($\lambda > 420$ nm) $BiVO_4$ electrode has a strong absorption. The band gap of the synthesized $BiVO_4$, calculated by using the Tauc plot, is 2.53 eV (Fig. 1d) and the result is comparable with the reported band gap of $BiVO_4$ [36,39].

3.2. PEC degradation of methyl orange with/without the addition of sulfite

The PEC degradation of MO is shown in Fig. 2. Without sulfite, the MO was degraded by only 10.9% after 2 h, while 50% of MO was degraded in the presence of 4 mM sulfite. With the increased of sulfite concentration, 73.1% and 96.6% MO degradation were observed with 8 mM and 16 mM sulfite addition, respectively. It shows that sulfite takes part in the degradation of MO and the degradation rate of MO was significantly increased as increasing the concentration of sulfite (Fig. 2a). As shown in Fig. 2b, the UV–vis absorption band (464 nm) of MO solution shows a quick decline in the presence of $BiVO_4$ and 16 mM sulfite under light irradiation. There was no shift of absorption band and no new emergence of absorption band was detected. UV–vis absorption result shows that the MO was fully degraded and there was no chromophoric molecule detected. The UV–vis absorption of MO solution under PEC/$BiVO_4$ with different concentration of sulfite are shown in Figure S1. To further evaluate the degradation kinetics, the rate constant of pseudo-first-order was calculated by using linearized regression and first decay model order ($-\ln(C/C_0) = kt$, Fig. 2c), where C_0 is the initial concentration of MO, C is the final concentration after light irradiation for a definite time period "*t*" and "*k*" is the rate constant. Fig. 2d shows that the rate constant enhances with the sulfite addition in the studied sulfite concentration range. With the addition of 4, 8, and 16 mM sulfite, the rate constant increased by about 6, 11, and ~30 times, respectively. The degradation rate constant was greatly improved due to the addition of sulfite.

The effect of the applied potential is further investigated. The degradation rates of MO are enhanced at all applied voltage with the addition of sulfite (Figure S2). After the addition of 16 mM sulfite, the degradation rates are increased by 16, 13, 12, 10 and ~30 times at applied voltage of 0 V, 0.5 V, 1 V, 1.5 V and 2 V vs. Ag/AgCl, respectively. The Linear Sweep Voltammograms (LSV) curves of $BiVO_4$ in MO solution (10 ppm) with different concentration of Na_2SO_3 were shown in Figure S3, it is found that the photocurrent is greatly enhanced after addition of sulfite, suggesting much faster redox reaction taking place on the electrode surface.

HPLC was used to analyze the PEC treated MO solution with and without sulfite. The result (Figure S4) shows that the retention time of MO moves forward which indicates the presence of other small intermediate molecules obtained from MO degradation during the PEC process which was later confirmed by the LC–MS. Further, the HPLC result shows that the $BiVO_4$ photoelectrode shows a high performance of photodegradation of MO with the addition of sulfite via the PEC process. The $BiVO_4$ film takes part in MO decolorization and degradation but it may not cause the mineralization of intermediates. The mineralization depends on the obstinacy of intermediate compounds. It is obvious that the decolorization rate was speedier than the mineralization rate of MO.

3.3. Sulfite-enhanced photo-electrocatalysis mechanism

Understanding the mechanism of sulfite-enhanced PEC MO degradation will help to use this approach for wide photo-electrocatalytic implementation. The reactive species are then studied by radical scavenging experiments, Electron Spin Resonance, Transient Absorption and so on.

The scavenging experiments are designed based on previous work by Li and co-workers [41]. Sodium sulfite has been widely used as a bleaching agent due to its sacrificial properties. It has a hole scavenging ability under light irradiation [44–46]. However, as shown in Fig. 3, adding hole scavengers such as EDTA did not enhance the degradation, indicating the enhancement is not due to the hole scavenging effect. $NaNO_3$, as an electron scavenger, was added to study the possible effect of aqueous electrons in the system. It is observed that the existence of

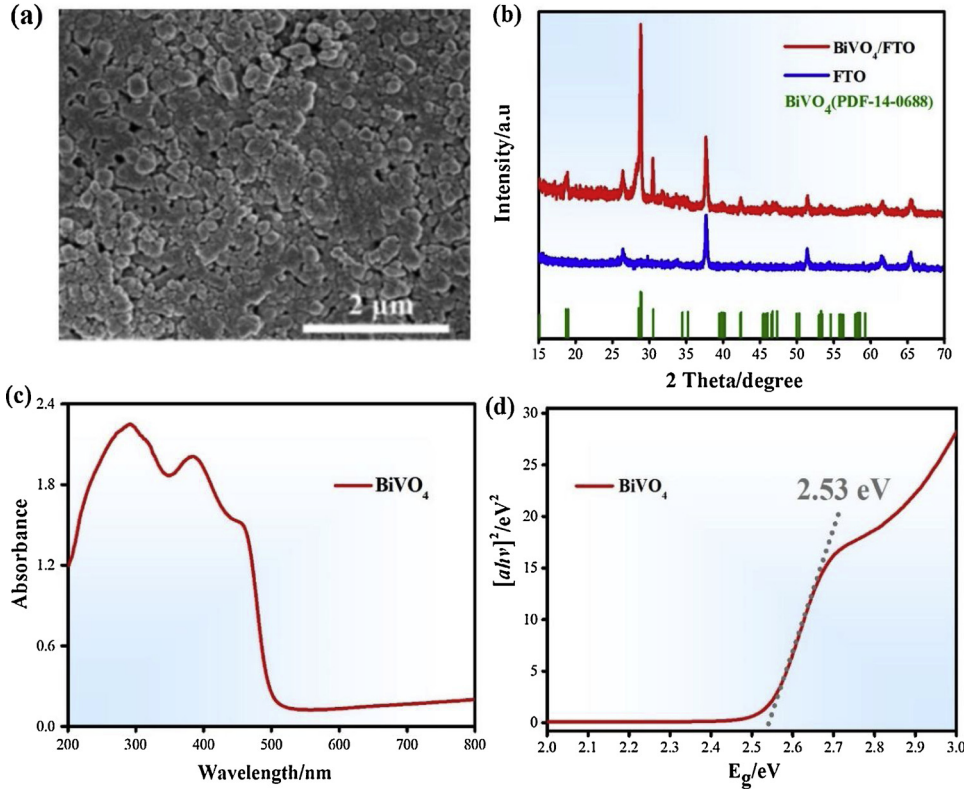

Fig. 1. (a) SEM image of the photoelectrode $BiVO_4$ nanoporous film on FTO substrate (b) XRD patterns of the naked FTO and nanoporous $BiVO_4$ film (c) UV–vis absorption spectrum of $BiVO_4$ (d) The Tauc plot of the $BiVO_4$ nanoporous film.

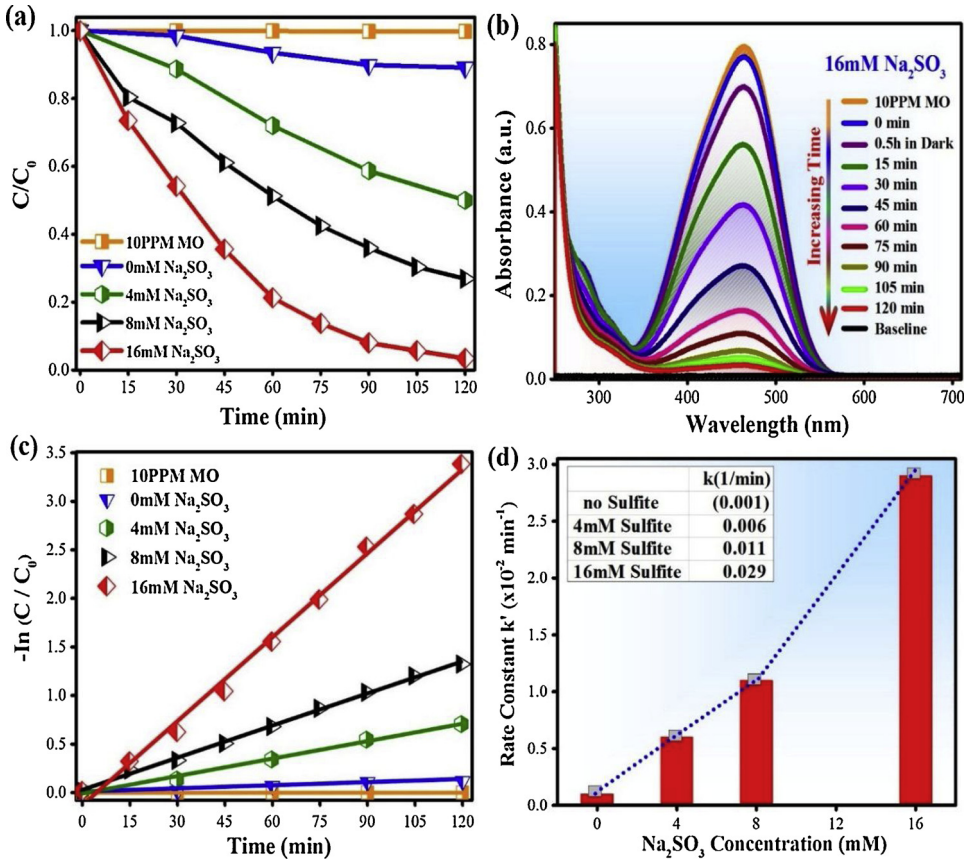

Fig. 2. (a) PEC degradation of MO at 2 V with and without Na_2SO_3 (b) Time-resolved UV–vis absorption of MO solution under visible light with $BiVO_4$ and 16 mM Na_2SO_3 (The initial concentration of MO was 10 ppm) (c) Kinetic fitting (d) The reliance of MO degradation rate constant on the concentration of sulfite.

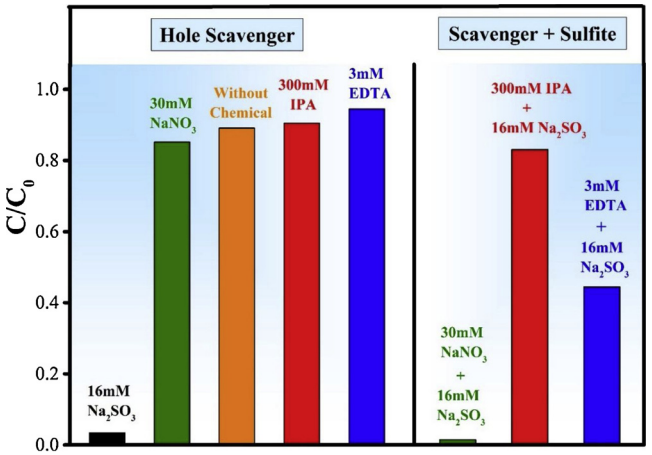

Fig. 3. The percentage of MO concentration left after 2-hour PEC degradation in the presence and absence of various scavengers.

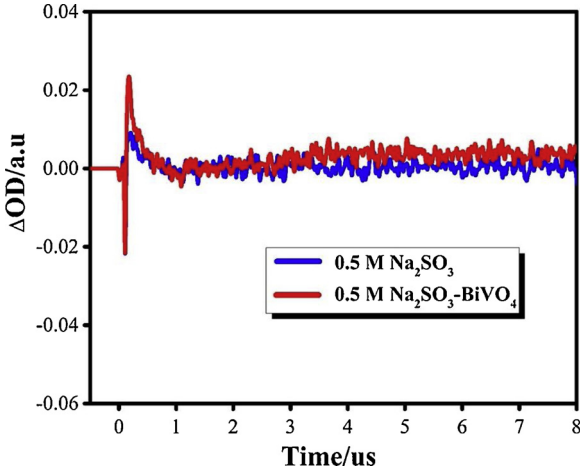

Fig. 5. Transient absorption spectra over 0.5 M Na_2SO_3 with and without $BiVO_4$ at 250 nm wavelength.

$NaNO_3$ did not influence the accelerated degradation of MO with sulfite addition, suggesting that degradation is not due to the aqueous electrons. However, the addition of IPA (scavengers for holes and hydroxyl radicals) almost fully retard the degradation of MO by $BiVO_4$ with the existence of sulfite. Therefore, it is proposed that holes and hydroxyl radicals are important for the PEC degradation of MO or the formation of other reactive species such as sulfite radical.

There are probably two pathways for the generation of $SO_3^{\bullet-}$ in the PEC system and the amount of $SO_3^{\bullet-}$ approximately doubled in whole photoelectrocatalytic reaction. In the first pathway, sulfite anion can be directly oxidized by photoinduced holes (Eq. 2). After one-electron removal of sulfite anion, $SO_3^{\bullet-}$ was obtained, which is a stronger oxygen depleting agent than SO_3^{2-}. This is possible because the redox potential of $SO_3^{\cdot-}/SO_3^{2-}$ couple is 0.75 V (vs NHE, at pH = 7) [47], which is less positive than the $BiVO_4$, VB potential (2.79 V) [48].

$$BiVO_4 \xrightarrow{hv} h^+ + e^- \quad (1)$$

$$h^+ + SO_3^{2-} \rightarrow SO_3^{\bullet-} \quad (2)$$

In the second pathway sulfite radical is produced through the reaction of sulfite anion with hydroxyl radicals (˙OH) (Eqs. 3 and 4) [49]. This is also possible since the redox potential of $^{\bullet}OH/OH^-$ (2.18 V vs NHE, at pH = 7) [50] is more positive than that of $SO_3^{\bullet-}/SO_3^{2-}$ (0.75 V):

$$h^+ + H_2O \rightarrow {}^{\bullet}OH + H^+ \quad (3)$$

$$^{\bullet}OH + SO_3^{2-} \rightarrow SO_3^{\bullet-} + OH^- \quad (4)$$

This can explain why the addition of scavengers for holes and hydroxyl radicals almost fully retard the PEC degradation of MO by $BiVO_4$ with the existence of sulfite. The radical scavenging results suggest that sulfite radical is a reactive agent produced from holes and hydroxyl radicals which may play a key role in MO degradation.

ESR experiment was then employed to measure the active species during the MO degradation. The ESR data (Fig. 4a) shows that without sulfite addition only DMPO -$^{\bullet}OH$ signals (aN = 15.2 G, a_{β}^{H} = 15.2 G) were detected in the $BiVO_4$ suspension. However, when sulfite is added, signals of DMPO-$SO_3^{\cdot-}$ adducts (aN = 14.7 G, a_{β}^{H} = 16.05 G) [51] were observed clearly (Fig. 4b). The intensity of DMPO-$SO_3^{\cdot-}$ were also increased with reaction time. The ESR results show a direct evidence of the generation of sulfite radical in the $BiVO_4$/sulfite system under light irradiation.

To further confirm the generation of $SO_3^{\bullet-}$, transient absorption spectra are investigated. The transient absorption peak at 250 nm can be assigned to sulfite radical ($SO_3^{\bullet-}$) according to reported work [52]. Fig. 5 presents the measured transient absorption decay spectra at 250 nm of the Na_2SO_3 solution or $BiVO_4$/sulfite suspension. The transient absorption confirms the generation of sulfite radical in the $BiVO_4$/sulfite system. In addition, the peak intensity of $BiVO_4$/sulfite suspension was much stronger than the sulfite solution, suggesting that more $SO_3^{\bullet-}$ generated after the $BiVO_4$ powder was introduced into the Na_2SO_3 solution. The mechanism of laser flash photolysis was discussed

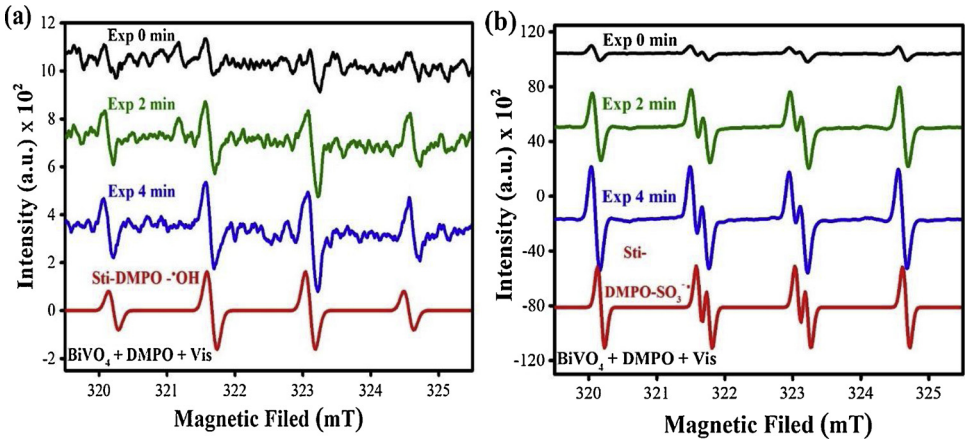

Fig. 4. ESR spectra of radicals trapped by DMPO after 4 min of light irradiation **(a)** $BiVO_4$ without sulfite (a_N = 15.2 G, a_B^H; = 15.2 G Line width = 0.89 G) **(b)** $BiVO_4$ with sulfite (a_N = 14.7 G, a_B^H; = 16.05 G Line width = 0.6 G). (Red curves are the simulated spectra).

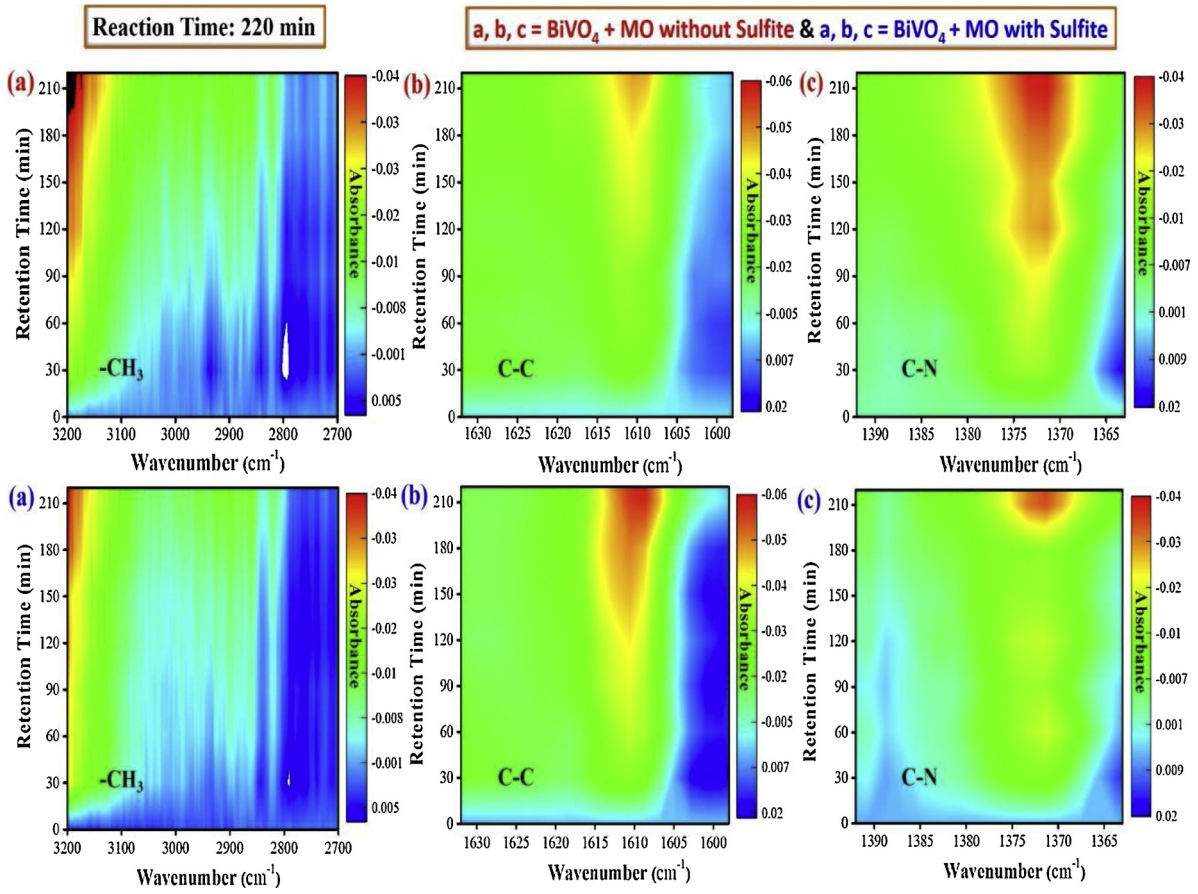

Fig. 6. DRIFT spectra of $BiVO_4$/MO with and without Na_2SO_3.

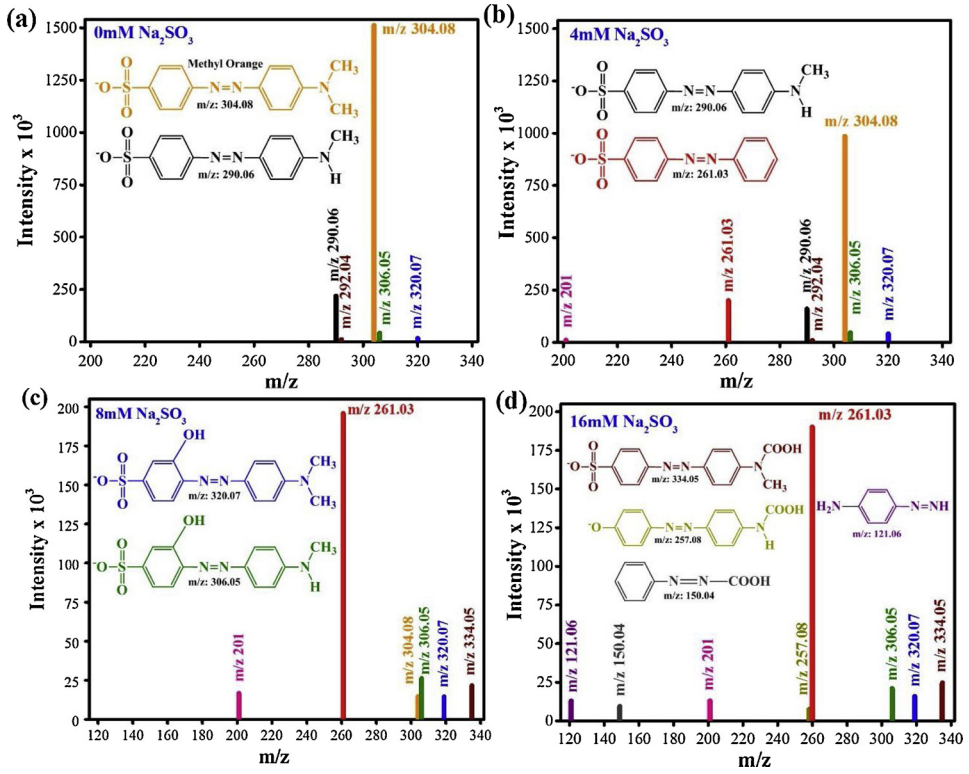

Fig. 7. LC–MS: Products after 2 h PEC degradation of MO **(a)** without addition of Na_2SO_3 **(b)** with 4 mM Na_2SO_3 **(c)** with 8 mM Na_2SO_3 and **(d)** with 16 mM Na_2SO_3.

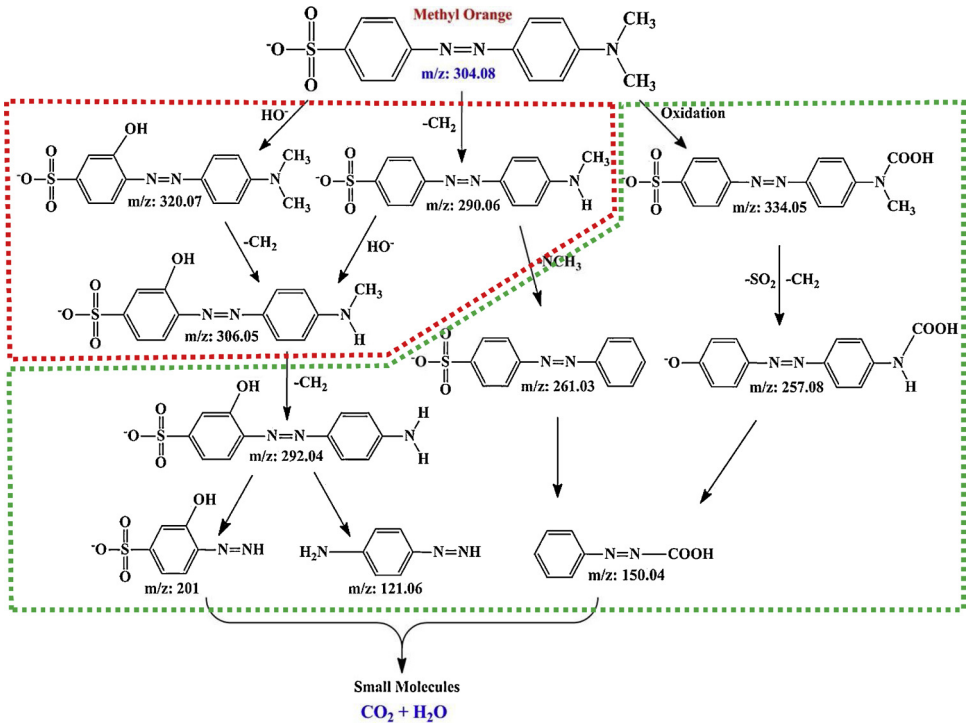

Fig. 8. The proposed Schematic demonstration of the PEC degradation pathway of MO. (Red dot line: main products without sulfite; Green dot line: main products with sulfite addition).

below:

$$SO_3^{2-} \xrightarrow{hv} SO_3^{\bullet -} + e_{aq}^- \quad (5)$$

Without $BiVO_4$ the generation of sulfite radical is shown in Eq. (5). When $BiVO_4$ was introduced into the system, the photocatalyst would generate hole-electron pairs under excitation as shown in Eq. (1). The photoinduced holes react with SO_3^{2-} and H_2O to produce sulfite radical and hydroxyl groups, and the hydroxyl groups participate in the Eq. (4). Therefore, more sulfite radicals were generated after introducing $BiVO_4$, which was beneficial for MO degradation.

3.4. Degradation pathway of methyl orange

An *in-situ* DRIFTS study was done to understand the mechanism of the sulfite-enhanced photochemical degradation process of MO. For this purpose, the DRIFT spectra of $BiVO_4$ /MO with and without the presence of sulfite was recorded. The DRIFT spectra of MO have three main broadband at 1370 cm^{-1} and 1380 cm^{-1} which is due to C—N bond, the bands at 1600 cm^{-1} to 1620 cm^{-1} are due to C—C bond and the band appears from 2800 cm^{-1} to 3100 cm^{-1} was due to C–H bond (Fig. 6a, b and Figure S5). The band at 1600 cm^{-1} to 1620 cm^{-1} was due to aromatic ring C—C bond [53] and also due to stretching vibration of carbonyl, ester, carboxyl and lactone groups [54,55]. The bands in the range of 1300-1400 $cm^{-1}$are assigned to the bend vibration of aromatic rings [56]. Fig. 6 shows that the bands intensity corresponding to C—H, C—N, and C—C bond decreases during the degradation process, which is due to the break of an azo group of MO molecule in the degradation process. The smashing of the C—C bond is much faster with the existence of sulfite, suggesting that the sulfite radical may accelerate the cleavage of an aromatic ring C—C bond.

To further understand the degradation pathway of MO, Q-Tof LC—MS analysis of the products obtained after 2 h PEC degradation was performed. The MS profile and the possible structures of the fragments are shown in Fig. 7. The red dot line encloses the main products without sulfite addition. Without the addition of sulfite, some of the parent molecules MO at *m/z* 304.08 disintegrates into a fragment with *m/z* value at 290.06 (Fig. 7a). The molecule structure of *m/z* value at 290.06 is provided in the inset of (Fig. 7a) as well. This is a demethylation process. The signal of MO is still strong, indicating the slow degradation process. However, with the sulfite addition (main products are shown inside the green dot line), for example at 16 mM sulfite added, the parent molecule MO at *m/z* 304.08 completely disintegrates into several fragments with a main one of *m/z* value at 261.03 (Fig. 7d). This is due to a cleavage of C—N bond in MO molecule [57–59]. Some other smaller molecules are also detected. The fragment with *m/z* value at 320.07 has a longer retention time and this intermediate compound are formed due to the demethylation and hydroxylation of MO [60]. The demethylation of MO is a procedure which includes the homolytic separation of the nitrogen-carbon bond of the amine group causing the replacement of a methyl group with a hydrogen atom. It was affirmed that intermediate with *m/z* value 320.07 was a mono hydroxylated MO. The product with *m/z* value 290.06 and *m/z* 292.04 was formed by cleaving of a methyl group from the MO molecule [60,61]. The intermediate compounds with *m/z* value 306.05 [61], and *m/z* value 290.06 are the by-products formed by the addition or by the cleavage of one or two hydroxyl groups or methylene groups. For example, a product with *m/z* value 306.05 is a derivative formed due to the decarboxylation also formed due to the addition of hydroxyl group from *m/z* value 290.06. It has been reported in the literature that intermediates of degraded methyl orange are less toxic and mineralized with time [62]. The intermediate with *m/z* values 261.03 was formed due to the removal of one nitrogen group and one methyl group. Further, azo bond (—N=N—) cleavage produces three intermediates with *m/z* value 201, *m/z* value 150.04 and *m/z* value 121.06 [61]. The intermediate with *m/z* value 150.04 was formed due to a further cleavage of the aromatic ring C—C bond, which is not observed in the case without sulfite, indicating that the sulfite radical can promote the aromatic ring C—C bond cleavage, in accordance with the *in-situ* DRIFTS observation. The LC—MS result suggested that the intermediates undergo a series of reactions such as the aromatic ring cleavage, demethylation, hydroxylation, decarboxylation and further mineralization. A degradation pathway is thus proposed in Fig. 8. The sulfite addition clearly accelerates the bonds

cleavage and leading to much faster degradation of MO.

4. Conclusions

In this paper, we demonstrate that PEC degradation of MO was significantly accelerated after sulfite addition. DRIFTs, transient absorption, ESR and hole scavenger studies show that sulfite radical plays a key role in the PEC degradation of MO. The degradation rate of MO was increased by almost 30 times with the addition of 16 mM Sulfite. Sulfite reacts with holes or hydroxyl radicals and forms the sulfite radicals, which were detected and proposed as a reactive species for the MO degradation. Sulfite-enhanced PEC degradation of MO has been successfully demonstrated in this paper, it was found that the sulfite radicals can accelerate C—C and C–N bonds cleavage in MO. This work provides a sustainable method for the beneficial use of air pollutants for the removal of water pollutants.

Notes

The authors declare no competing financial interest.

Acknowledgments

The authors gratefully acknowledge financial support from Ministry of Science and Technology of the People's Republic of China (2016YFE0112200 and 2016YFC0202700), and National Natural Science Foundation of China (No. 21677037, No. 21507011 and No. 21607027).

Appendix A. Supplementary data

Supplementary material related to this article can be found, in the online version, at doi:https://doi.org/10.1016/j.apcatb.2019.02.049.

References

[1] S.P. Ghuge, A.K. Saroha, Catalytic ozonation for the treatment of synthetic and industrial effluents-application of mesoporous materials: a review, J. Environ. Manage. 211 (2018) 83–102.
[2] W. Liu, W. Hu, J. Liu, Study on the photoreductive decolorization of azo dyes by sulfite aqua, AIP Conference Proceedings (2017) 050006.
[3] J. Wang, H. Li, S. Meng, L. Zhang, X. Fu, S. Chen, One-pot hydrothermal synthesis of highly efficient SnOx/Zn_2SnO_4 composite photocatalyst for the degradation of methyl orange and gaseous benzene, Appl. Catal. B 200 (2017) 19–30.
[4] S. Rasalingam, R. Peng, R.T. Koodali, Removal of hazardous pollutants from wastewaters: applications of TiO_2-SiO_2 mixed oxide materials, J. Nanomater. 2014 (2014) 10.
[5] H. Geng, P. Du, Z. Zhang, L. Yao, K. Cao, S. Li, P. Sheng, Architecting Bi_2S_3/graphene quantum dots/TiO_2 photoelectrodes for aqueous Cr (VI)/methyl orange removal, Mater. Lett. 214 (2018) 146–149.
[6] C. Umamaheswari, A. Lakshmanan, N. Nagarajan, Green synthesis, characterization and catalytic degradation studies of gold nanoparticles against congo red and methyl orange, J. Photochem. Photobiol. B, Biol. 178 (2018) 33–39.
[7] A.A. Mansur, H.S. Mansur, F.P. Ramanery, L.C. Oliveira, P.P.J.A.C.B.E. Souza, "Green" colloidal ZnS quantum dots/chitosan nano-photocatalysts for advanced oxidation processes: study of the photodegradation of organic dye pollutants, 158 (2014) 269-279.
[8] F. Zhang, G. Dong, M. Wang, Y. Zeng, C. Wang, Efficient removal of methyl orange using Cu_2O as a dual function catalyst, Appl. Surf. Sci. 444 (2018) 559–568.
[9] J. Grzechulska, A.W. Morawski, Photocatalytic decomposition of azo-dye acid black 1 in water over modified titanium dioxide, Appl. Catal. B 36 (2002) 45–51.
[10] I. Ali, M. Asim, T.A. Khan, Low cost adsorbents for the removal of organic pollutants from wastewater, J. Environ. Manage. 113 (2012) 170–183.
[11] M. Megharaj, B. Ramakrishnan, K. Venkateswarlu, N. Sethunathan, R. Naidu, Bioremediation approaches for organic pollutants: a critical perspective, Environ. Int. 37 (2011) 1362–1375.
[12] C. Comninellis, Electrocatalysis in the electrochemical conversion/combustion of organic pollutants for waste water treatment, Electrochim. Acta 39 (1994) 1857–1862.
[13] Y. Feng, L. Ling, Y. Wang, Z. Xu, F. Cao, H. Li, Z.J.N.E. Bian, Engineering spherical lead zirconate titanate to explore the essence of piezo-catalysis, Nano Energy 40 (2017) 481–486.
[14] G.-d. Kang, Y.-m. Cao, Development of antifouling reverse osmosis membranes for water treatment: a review, Water Res. 46 (2012) 584–600.
[15] M. Rauf, S.S. Ashraf, Fundamental principles and application of heterogeneous photocatalytic degradation of dyes in solution, Chem. Eng. J. 151 (2009) 10–18.
[16] Y. Feng, H. Li, L. Ling, S. Yan, D. Pan, H. Ge, H. Li, Z. Bian, Enhanced photocatalytic degradation performance by fluid-induced piezoelectric field, Environ. Sci. Technol. 52 (2018) 7842–7848.
[17] C. Barrera-Díaz, I. Linares-Hernández, G. Roa-Morales, B. Bilyeu, P. Balderas-Hernández, Removal of biorefractory compounds in industrial wastewater by chemical and electrochemical pretreatments, Ind. Eng. Chem. Res. 48 (2008) 1253–1258.
[18] K. Sharma, B. Rao, H. Mohan, J. Mittal, J. Oakes, P. O'Neill, Free-radical-induced oxidation and reduction of 1-arylazo-2-naphthol dyes: a radiation chemical study, J. Phys. Chem. A 106 (2002) 2915–2923.
[19] M. Canterino, I. Di Somma, R. Marotta, R. Andreozzi, V. Caprio, Energy recovery in wastewater decontamination: simultaneous photocatalytic oxidation of an organic substrate and electricity generation, Water Res. 43 (2009) 2710–2716.
[20] V.M. Daskalaki, I. Fulgione, Z. Frontistis, L. Rizzo, D. Mantzavinos, Solar light-induced photoelectrocatalytic degradation of bisphenol-A on TiO_2/ITO film anode and BDD cathode, Catal. Today 209 (2013) 74–78.
[21] X. Chen, L. Liu, Y. Feng, L. Wang, Z. Bian, H. Li, Z.L. Wang, Fluid eddy induced piezo-promoted photodegradation of organic dye pollutants in wastewater on ZnO nanorod arrays/3D Ni foam, Mater. Today 20 (2017) 501–506.
[22] V.K. Gupta, R. Jain, A. Nayak, S. Agarwal, M. Shrivastava, Removal of the hazardous dye—tartrazine by photodegradation on titanium dioxide surface, Mater. Sci. Eng. C 31 (2011) 1062–1067.
[23] J.H. Park, S. Kim, A.J. Bard, Novel carbon-doped TiO_2 nanotube arrays with high aspect ratios for efficient solar water splitting, Nano Lett. 6 (2006) 24–28.
[24] M. Xu, Y. Chen, J. Qin, Y. Feng, W. Li, W. Chen, J. Zhu, H. Li, Z. Bian, Unveiling the role of defects on oxygen activation and photodegradation of organic pollutants, Environ. Sci. Technol. 52 (2018) 13879–13886.
[25] L. Xiang, X. Zhao, Wet-chemical preparation of TiO_2-based composites with different morphologies and photocatalytic properties, Nanomaterials 7 (2017) 310.
[26] Y. Zhang, M. Xu, H. Li, H. Ge, Z. Bian, The enhanced photoreduction of Cr (VI) to Cr (III) using carbon dots coupled TiO_2 mesocrystals, Appl. Catal. B 226 (2018) 213–219.
[27] L. Ling, L. Liu, Y. Feng, J. Zhu, Z. Bian, Synthesis of TiO_2 mesocrystal film with enhanced photocatalytic activity, Chin. J. Catal. 39 (2018) 639–645.
[28] J. Lu, Q. Meng, H. Lv, L. Shui, M. Jin, Z. Zhang, Z. Chen, M. Yuan, X. Wang, J.-M. Liu, Synthesis of visible-light-driven BiOBrxI1-x solid solution nanoplates by ultrasound-assisted hydrolysis method with tunable bandgap and superior photocatalytic activity, J. Alloys. Compd. 732 (2018) 167–177.
[29] D. Jiang, J. Li, C. Xing, Z. Zhang, S. Meng, M. Chen, Two-dimensional $CaIn_2S_4$/g-C_3N_4 heterojunction nanocomposite with enhanced visible-light photocatalytic activities: interfacial engineering and mechanism insight, ACS Appl. Mater. Interfaces 7 (2015) 19234–19242.
[30] G. Rao, H. Zhao, J. Chen, W. Deng, B. Jung, A. Abdel-Wahab, B. Batchelor, Y. Li, FeOOH and Fe_2O_3 co-grafted TiO_2 photocatalysts for bisphenol A degradation in water, Catal. Commun. 97 (2017) 125–129.
[31] T. Xu, L. Zhang, H. Cheng, Y. Zhu, Significantly enhanced photocatalytic performance of ZnO via graphene hybridization and the mechanism study, Appl. Catal. B 101 (2011) 382–387.
[32] L. Zhang, T. Xu, X. Zhao, Y. Zhu, Controllable synthesis of Bi_2MoO_6 and effect of morphology and variation in local structure on photocatalytic activities, Appl. Catal. B 98 (2010) 138–146.
[33] Y. Feng, L. Ling, J. Nie, K. Han, X. Chen, Z. Bian, H. Li, Z.L. Wang, Self-powered electrostatic filter with enhanced photocatalytic degradation of formaldehyde based on built-in triboelectric nanogenerators, ACS Nano 11 (2017) 12411–12418.
[34] W. David, I. Wood, Ferroelastic phase transition in $BiVO_4$: VI. Some comments on the relationship between spontaneous deformation and domain walls in ferroelastics, J. Phys. C Solid State Phys. 16 (1983) 5149.
[35] K. Hirota, G. Komatsu, M. Yamashita, H. Takemura, O. Yamaguchi, Formation, characterization and sintering of alkoxy-derived bismuth vanadate, Mater. Res. Bull. 27 (1992) 823–830.
[36] L. Zhang, C.Y. Lin, V.K. Valev, E. Reisner, U. Steiner, J.J. Baumberg, Plasmonic enhancement in $BiVO_4$ photonic crystals for efficient water splitting, Small 10 (2014) 3970–3978.
[37] Y. Feng, H. Cheng, J. Han, X. Zheng, Y. Liu, Y. Yang, L. Zhang, Chlorophyll sensitized $BiVO_4$ as photoanode for solar water splitting and CO_2 conversion, Chin. Chem. Lett. 28 (2017) 2254–2258.
[38] L. Zhang, L.O. Herrmann, J.J. Baumberg, Size dependent plasmonic effect on $BiVO_4$ photoanodes for solar water splitting, Sci. Rep. 5 (2015) 16660.
[39] J. Han, X. Zheng, L. Zhang, H. Fu, J. Chen, Removal of SO_2 on a nanoporous photoelectrode with simultaneous H_2 production, Environ. Sci. Nano 4 (2017) 834–842.
[40] Q. Pan, C. Zhang, Y. Xiong, Q. Mi, D. Li, L. Zou, Q. Huang, Z. Zou, H. Yang, Boosting charge separation and transfer by plasmon-enhanced MoS_2/$BiVO_4$ p–n heterojunction composite for efficient photoelectrochemical water splitting, ACS Sustain. Chem. Eng. 6 (2018) 6378–6387.
[41] W. Deng, H. Zhao, F. Pan, X. Feng, B. Jung, A. Abdel-Wahab, B. Batchelor, Y. Li, Visible-light-driven photocatalytic degradation of organic water pollutants promoted by sulfite addition, Environ. Sci. Technol. 51 (2017) 13372–13379.
[42] L. Chen, W. Ding, F. Wu, Comment on "Visible-Light-Driven photocatalytic degradation of organic water pollutants promoted by sulfite addition", Environ. Sci. Technol. 52 (2018) 1675–1676.
[43] Y. Yang, L. Liu, H. Yin, D. Xu, G. Liu, X. Song, J. Liu, White light assisted photosensitized synthesis of Ag nanoparticles: excited-state hydrogen bonding roles, J. Phys. Chem. C 117 (2013) 11858–11865.
[44] J. Li, S.K. Cushing, P. Zheng, T. Senty, F. Meng, A.D. Bristow, A. Manivannan,

N. Wu, Solar hydrogen generation by a CdS-Au-TiO_2 sandwich nanorod array enhanced with Au nanoparticle as electron relay and plasmonic photosensitizer, J. Am. Chem. Soc. 136 (2014) 8438–8449.
[45] F.A. Frame, E.C. Carroll, D.S. Larsen, M. Sarahan, N.D. Browning, F.E. Osterloh, First demonstration of CdSe as a photocatalyst for hydrogen evolution from water under UV and visible light, Chem. Commun. (2008) 2206–2208.
[46] F.E. Osterloh, Nanoparticle-assembled catalysts for photochemical water splitting, On Solar Hydrogen &Nanotechnol. (2010) 507–521.
[47] T.N. Das, R.E. Huie, P. Neta, Reduction potentials of $SO_3^{\bullet -}$, $SO_5^{\bullet -}$, and $S_4O_6^{\bullet 3-}$ radicals in aqueous solution, J. Phys. Chem. A 103 (1999) 3581–3588.
[48] T. Saison, P. Gras, N. Chemin, C. Chanéac, O. Durupthy, V. Brezová, C. Colbeau-Justin, J.-P. Jolivet, New insights into Bi_2WO_6 properties as a visible-light photocatalyst, J. Phys. Chem. C 117 (2013) 22656–22666.
[49] P. Neta, R.E. Huie, Free-radical chemistry of sulfite, Environ. Health Perspect. 64 (1985) 209.
[50] W. Koppenol, J. Butler, Energetics of interconversion reactions of oxyradicals, Adv. Free. Radic. Biol. Med. 1 (1985) 91–131.
[51] K. Ranguelova, A.B. Rice, A. Khajo, M. Triquigneaux, S. Garantziotis, R.S. Magliozzo, R.P. Mason, Formation of reactive sulfite-derived free radicals by the activation of human neutrophils: an ESR study, Free Radic. Biol. Med. 52 (2012) 1264–1271.
[52] E. Hayon, A. Treinin, J. Wilf, Electronic spectra, photochemistry, and autoxidation mechanism of the sulfite-bisulfite-pyrosulfite systems. SO_2^-, SO_3^-, SO_4^-, and SO_5^- radicals, J. Am. Chem. Soc. 94 (1972) 47–57.
[53] T. Shen, C. Jiang, C. Wang, J. Sun, X. Wang, X. Li, A TiO_2 modified abiotic–biotic process for the degradation of the azo dye methyl orange, RSC Adv. 5 (2015) 58704–58712.
[54] S. Biniak, M. Pakuła, G. Szymański, A. Światkowski, Effect of activated carbon surface oxygen-and/or nitrogen-containing groups on adsorption of copper (II) ions from aqueous solution, Langmuir 15 (1999) 6117–6122.
[55] F.J. López-Garzón, M. Domingo-García, M. Pérez-Mendoza, P.M. Alvarez, V. Gómez-Serrano, Textural and chemical surface modifications produced by some oxidation treatments of a glassy carbon, Langmuir 19 (2003) 2838–2844.
[56] P. Alvarez, J. Garcia-Araya, F. Beltrán, F. Masa, F. Medina, Ozonation of activated carbons: effect on the adsorption of selected phenolic compounds from aqueous solutions, J. Colloid Interface Sci. 283 (2005) 503–512.
[57] C. Baiocchi, M.C. Brussino, E. Pramauro, A.B. Prevot, L. Palmisano, G. Marcì, Characterization of methyl orange and its photocatalytic degradation products by HPLC/UV–VIS diode array and atmospheric pressure ionization quadrupole ion trap mass spectrometry, Int. J. Mass Spectrom. 214 (2002) 247–256.
[58] R. Comparelli, E. Fanizza, M. Curri, P. Cozzoli, G. Mascolo, R. Passino, A. Agostiano, Photocatalytic degradation of azo dyes by organic-capped anatase TiO_2 nanocrystals immobilized onto substrates, Appl. Catal. B 55 (2005) 81–91.
[59] K. Dai, H. Chen, T. Peng, D. Ke, H. Yi, Photocatalytic degradation of methyl orange in aqueous suspension of mesoporous titania nanoparticles, Chemosphere 69 (2007) 1361–1367.
[60] Y. He, F. Grieser, M. Ashokkumar, The mechanism of sonophotocatalytic degradation of methyl orange and its products in aqueous solutions, Ultrason. Sonochem. 18 (2011) 974–980.
[61] J. Kaur, S. Singhal, Facile synthesis of ZnO and transition metal doped ZnO nanoparticles for the photocatalytic degradation of Methyl Orange, Ceram. Int. 40 (2014) 7417–7424.
[62] H. Trabelsi, M. Khadhraoui, O. Hentati, M. Ksibi, Titanium dioxide mediated photodegradation of methyl orange by ultraviolet light, Toxicol. Environ. Chem. 95 (2013) 543–558.